YMP Engineered Barrier Systems Scaled Ventilation Testing

Sandi Dalvit Dunn[a], Bill Lowry[a], Bob Walsh[a], John del Mar[a], Cliff Howard[b], Roy Johnston[b], Troy Williams[c]

[a]Science and Engineering Associates, Inc., Sante Fe, New Mexico 87507
[b]Sandia National Laboratories, Albuquerque, New Mexico 87185
[c]Lawrence Livermore National Laboratories, Livermore, California 94550
sdunn@seabase.com

Introduction

Yucca Mountain, approximately 100 miles northwest of Las Vegas, Nevada, has been selected as the site for the nation's first geologic repository for high level nuclear waste. The Yucca Mountain Project (YMP) is currently developing the design for the underground facilities. Ventilation is a key component of the design as a way to maintain the desired thermal conditions in the emplacement drifts prior to closure. As a means of determining the effects of continuous ventilation on heat removal from the emplacement drifts two series of scaled ventilation tests have been performed.

Both test series were performed in the DOE/North Las Vegas Atlas facility. The tests provided scaled (nominally 25% of the full scale emplacement drift design) thermal and flow process data that will be used to validate YMP heat and mass transport codes. The Phase I Ventilation Test series evaluated the ability of ambient ventilation air to remove energy under varying flow and input power conditions. The Phase II Ventilation Test series evaluated the ability of pre-conditioned ventilation air to remove energy under varying flow, input temperature and moisture content, and simulated waste package input power conditions. Twenty-two distinct ventilation tests were run.

Work Description

The tests were conducted in a 40.2-m-long, 1.37 m diameter, insulated concrete pipe test train, in which simulated waste packages fabricated from steel were placed to form a 33.9-m-long, 0.41 m diameter uniform heat source. Figure 1 shows a plan view of the test train (as

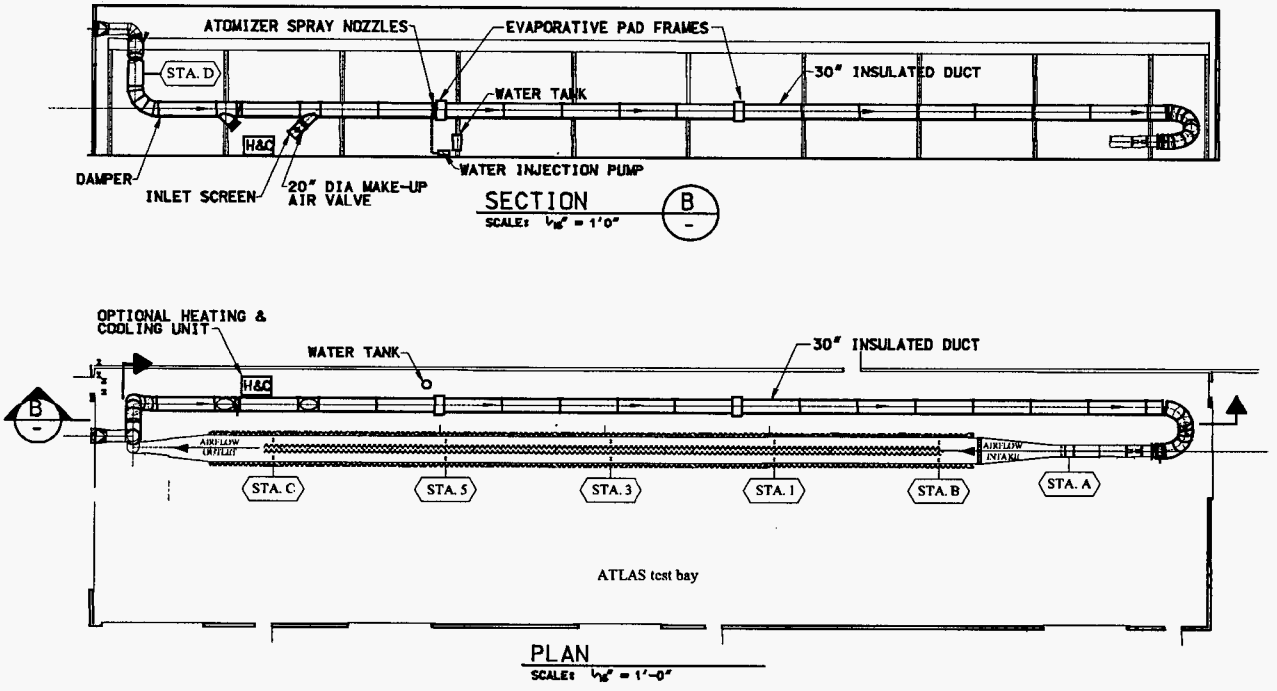

Figure 1: Plan view of the Atlas ventilation test facility, as configured for the Phase II Ventilation test series (Howard 2001a).

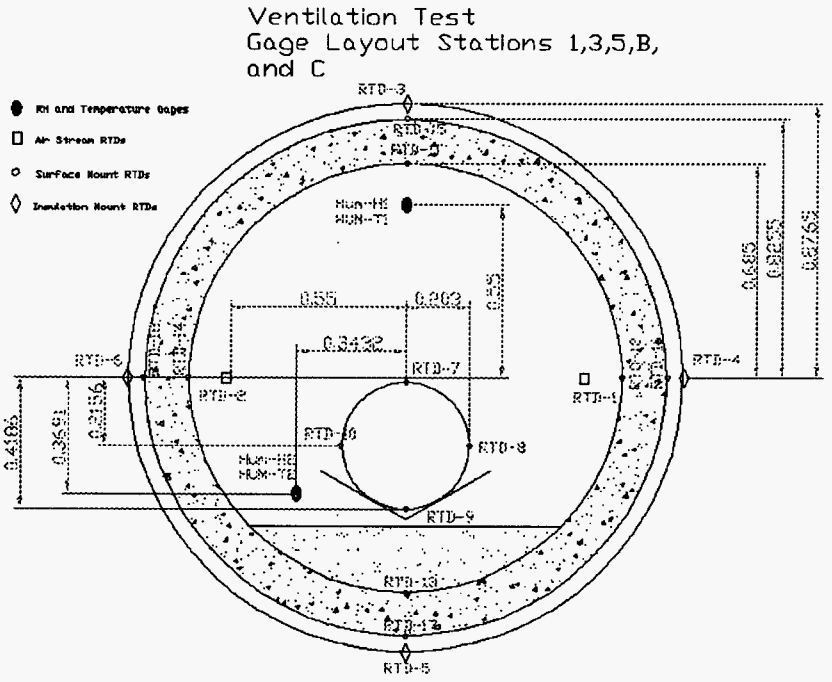

Figure 2: Cross sectional view of the sensor stations in the heated section of the test train (Howard 2001a).

configured for the Phase II tests). The waste packages were assembled on steel pallets that sat atop support rails. Single rod electrical heaters centered in the steel drums simulated the heat produced by the decaying waste. Crushed tuff was placed beneath the waste packages to form an invert. Ventilation air was moved through the test train with an axial fan system. Steel transition pieces were fabricated to connect the ventilation ducting to the test train. Figure 2 depicts a cross-sectional view of a typical station. The heated region extends between Stations B and C. The inlet (Station A) was open to the test bay for the Phase I tests, and was connected to a reconditioning loop for the Phase II tests. The outlet (Station D) was vented to the exterior of the building for the Phase I tests, and was connected to a reconditioning loop for the Phase II tests. Section B (Figure 1) shows the air-reconditioning loop added for the Phase II tests. Power input and ventilation airflow rates were varied in the test matrix for both the Phase I and Phase II tests. Additionally, the inlet ventilating air temperature and moisture content were controlled and varied as prescribed inlet conditions in the test matrix for the Phase II tests.

The Phase I test matrix stipulated six test conditions, varying power at two levels (180 and 360 W/m) and airflow rates from 0.5 to 3 m^3/sec. Each test was run to relatively steady conditions, requiring 6 to 10 days to complete. The test train was typically allowed to cool to ambient conditions prior to establishing new flow and heat input conditions for a subsequent test. Table 1 shows the test matrix.

The Phase II test matrix included sixteen test conditions, varying power at two levels (220 and 360 W/m), air flow rates of 0.5 and 1.0 m^3/sec, inlet air temperatures between 25 and 45 degree C, and inlet air relative humidity between 10 and 50 %RH (Table 2). Each test was run to relatively steady conditions, requiring 3 to 18 days to complete. The tests were divided into subsets based on the power level and inlet air volume. Each subset consisted of a suite of at least three tests varying only by air inlet conditions (temperature and relative humidity). The test train was typically allowed to cool to ambient conditions after each suite of tests in a subset was completed.

Table 1. Phase I Ventilation Test Conditions

Test Designation	Nominal Power Input (kW/m)	Nominal Flow (m^3/s)
Test 1 / Case 4	0.18	1
Test 2 / Case 5	0.18	0.5
Test 3 / Case 1	0.36	1
Test 4 / Case 2	0.36	2
Test 5 / Case 3	0.36	0.5
Test 6 / Case 6	0.36	3

Table 2. Phase II Ventilation Test Conditions

Test Designation	Inlet Air Conditions T (^{0}C)	RH (%)	Nominal Power Input (kW/m)	Nominal Flow (m^3/s)
Test 1	25	30	0.22	1
Test 2	35	17		
Test 3	45	10		
Test 4	45	15		
Test 5	25	30	0.36	1
Test 6	35	17		
Test 7	45	10		
Test 8	45	15		
Test 9	25	30	0.22	0.5
Test 10	35	17		
Test 11	45	17		
Test 12	25	30	0.36	0.5
Test 13	35	17		
Test 14	45	10		
Test 15	30	30	0.36	1
Test 16	30	49		

Ventilating airflow rate, temperature and relative humidity were measured at the inlet and outlet (Stations A and D). Heater power input was measured in five sections along the heated length of the test train. Each of the five measurement stations (B, 1, 3, 5, and C) along the length of the heated portion of the test train had surface mounted temperature sensors on each of the four quadrants of the test train (top, right, bottom, and left) on the exterior of the insulation, at the insulation/concrete interface, on the concrete interior, and on the waste package exterior (Figure 2). Additionally, each of these stations measured the ventilating air relative humidity and temperature at the crown of the test train and near the waste package as well as the air temperature along each side of the test train. In all, 80 surface temperatures, 24 air temperatures, and 14 relative humidity measurements were measured and automatically recorded at 15 minute intervals throughout the tests. Ambient pressure, temperature, and relative humidity measurements were also collected.

Results

The ventilation tests were executed over a total duration of approximately 12 months. In general, the tests were executed with few or no difficulties. Data is presented in its entirety in *Testing to Provide Data for Ventilation System Design: Phase I* (OCRWMS 2002a) and *Testing to Provide Data for Ventilation System Design: Phase II* (OCRWMS 2002b).

The airflow rate and waste package power input were very well controlled, providing stable conditions throughout the tests at the desired nominal set points. The flow rates for each test were calculated based on air velocity probe differential pressure, relative humidity, barometric pressure, and air temperature measurements. The total power input was the sum of the measured power input for each of the five power monitors along the test train. The average line load (energy), defined as the total measured power divided by the total heated length of the test train (33.9 m), was calculated from the data. Figures 3 and 4 show typical airflow rate and power/energy input histories.

For the Phase I tests, inlet air temperature varied by as much as 15C daily, due to the variation in the test bay temperature. This variation of inlet air temperature resulted in daily variation of all other temperatures in the test train by several degrees, having the greatest impact on the air,

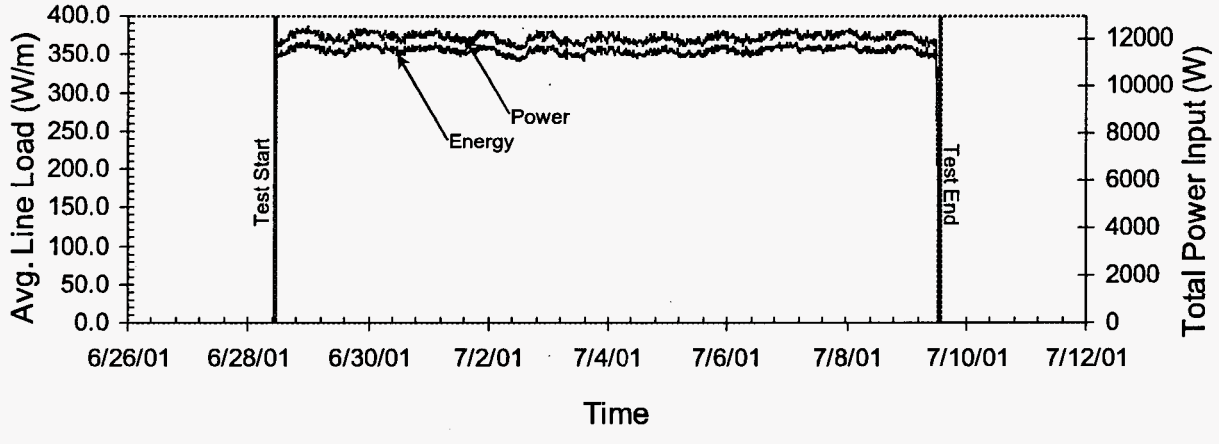

Figure 3: Measured total power input along with the average line load over the length of the test train (Phase II, Test 8)

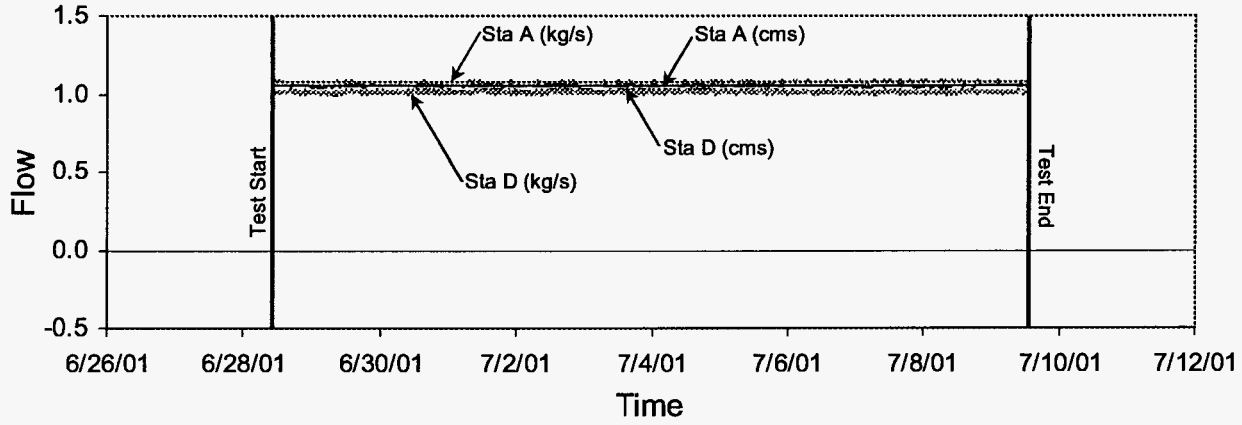

Figure 4: Calculated volumetric and mass flow rates at Stations A and D (Phase II, Test 8)

and decreasing impact on waste package and concrete temperatures, in that order. Figure 5 shows a typical history of the measured air temperature as a function of location along the test train for a Phase I test. For the Phase II tests, the conditioning loop provided a controlled and stable inlet air temperature. The moisture content of the inlet air was less stable, being influenced by changes in ambient conditions. The duration of most tests allowed for data to be collected at or near the desired nominal inlet air relative humidity after steady state conditions were reached.

A summary of the test data was compiled using averaged values. The averages were calculated over a representative period of time (24 hours) chosen as the last full day of data representative of the desired test conditions. To present a clear picture of temperatures within the experimental train, these data were then plotted as a function of axial and cross sectional position. Figures 6 and 7 show typical results.

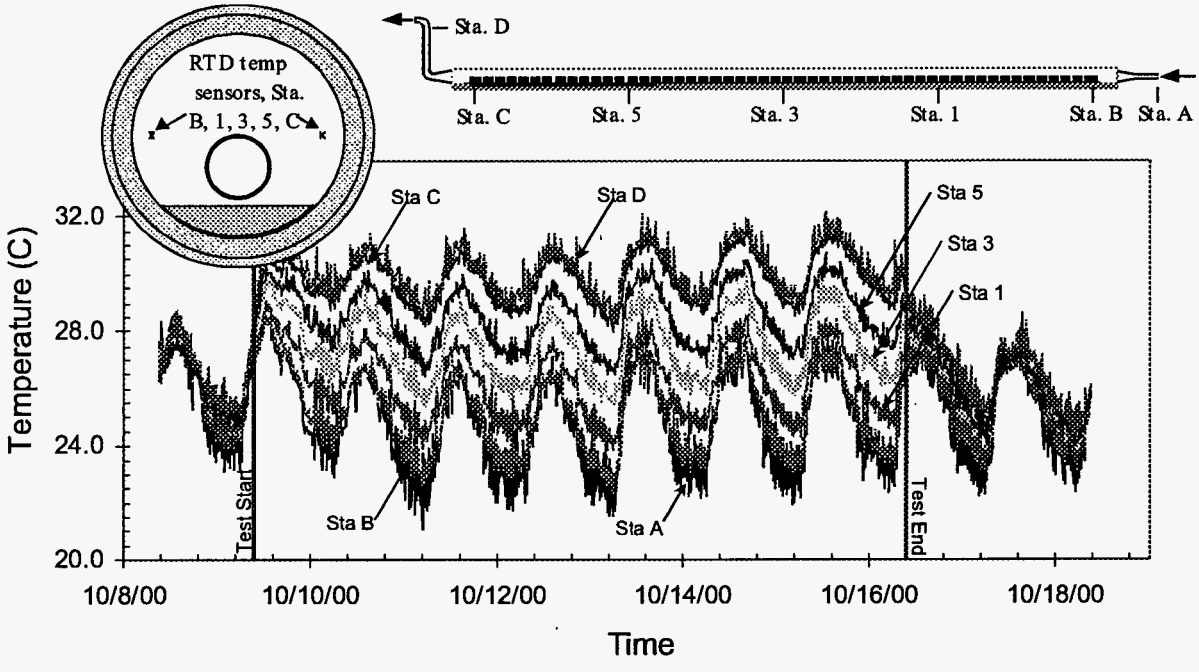

Figure 5: Measured air temperature at each Station along the length of the test train (Phase I, Test 1)

Review of these plots showed:

- The temperature of the ventilating air always increased with axial position throughout the heated region of the test train (Stations B through C). The air temperature was lower than both the interior of the concrete and the waste package for all stations except C due to radiative transfer of energy between the waste package and the interior surface of the concrete wall

- The profile of the axial temperature curves shows that the temperatures at a particular position increased with distance along the test train between the beginning of the heated Section and the centermost station (stations B and 3). For all surfaces but the waste package, the recorded temperatures also increased between stations 3 and 5. For the waste package a drop in temperature was seen between station 3 and the end of the test train (station C). For all other surfaces, a temperature drop was seen between station 5 and the end of the test train (station C). The decrease in temperatures near the end of the heated region of the test train are likely caused by end effects. This is a slight departure from the conceptual model of continuously increasing waste package temperature with distance, and is likely due to radiative end effects not considered in the original model.

- At a given station in the test train, the waste package surface was the hottest, followed by the concrete pipe internal surface, followed by the air. This is consistent with the conceptual model of both the waste package and the pipe wall transferring heat to the air.

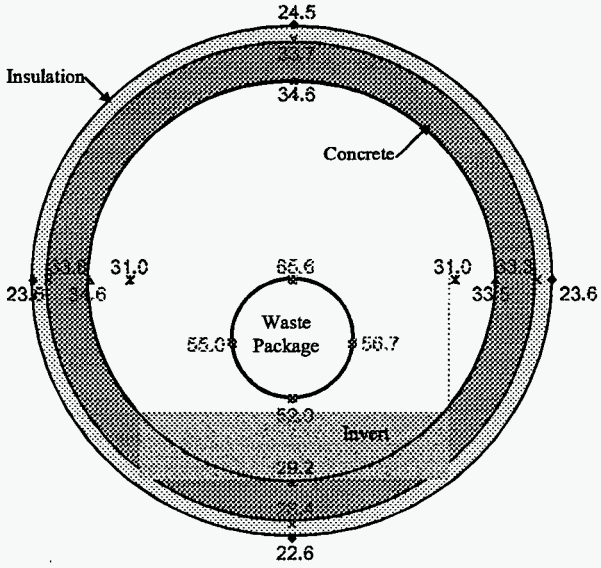

Figure 6: Cross-sectional view of the 24 hour average steady state temperatures for the centermost station (Sta. 3). (Phase I, Test 5).

- The circumferential temperature gradient was relatively large on the waste packages (as high as 13 C from the top to the bottom of the waste package), with the hottest temperatures at the top and coolest at the bottom of the waste package in all cases. This is due to the design of the waste package heater, where a single rod heating element was located in the center of the waste package,

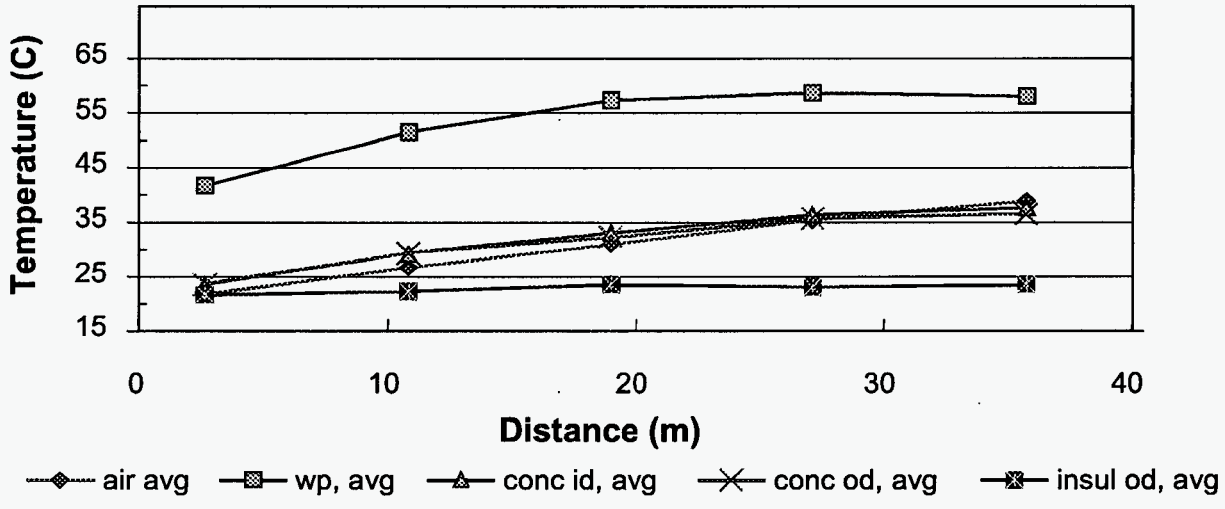

Figure 7: Calculated average temperatures for each surface along the length of the test train (Phase I, Test 5).

resulting in thermal stratification of air inside the package.

- The circumferential temperature gradient on the inner surface of the concrete pipe exposed to air was small, typically within 1 to 3C.

Data were used to determine how the various conditions affected the ability of the ventilating air to remove energy. Ventilation efficiency, defined as the percentage of the heat removed from the waste packages by the ventilating air, was calculated for each test based on the enthalpy change of the ventilating air. The change in the enthalpy of the air between the start and the end of the heated region of the test train represents the heat gained by the ventilating air. The mass flow rate of air and water vapor were calculated from the differential pressure gages, relative humidity gages, and air temperature measurements taken at the inlet, station A. Enthalpy values for air were interpolated directly from property tables based on the average measured air temperature at each station. The enthalpy of the water vapor contained in the air-water mixture was calculated based on the temperature and specific heat of water vapor.

Under the test conditions, the enthalpy changes (kJ/kg) of dry air and water vapor can be determined by (Çengel and Boles 1994):

$$\Delta h_{air} = 1.005(T_C - T_B)$$

$$\Delta h_{w.v.} = 2501.3 + 1.82T_C - (2501.3 + 1.82T_B) = 1.82(T_C - T_B)$$

where T_B and T_C are the temperatures at stations B and C.

The rate of energy transfer to the gas, $\dot{Q}$ (kJ/s), is (Çengel and Boles)

$$\dot{Q} = \dot{m}_{air}\Delta h_{air} + \dot{m}_{w.v.}\Delta h_{w.v.}$$

where $\dot{m}_{air}$ and $\dot{m}_{w.v.}$ are the mass flow rates (kg/s) of dry air and water vapor. This equation is simplified from the reference because no work was done on the air between Stations B and C and the mass flow rate is constant. The mass flow rates are

$$\dot{m}_{air} = f_{air}(16.018463\rho)\dot{V}$$

$$\dot{m}_{w.v.} = f_{w.v.}(16.018463\rho)\dot{V}$$

where f_{air} and $f_{w.v.}$ are the mass fractions of dry air and water vapor and $f_{air} + f_{w.v.} = 1$

$\dot{V}$ is the volumetric flow rate and ρ is the mixture density (lb/ft^3) at Station A, and 16.018463 is a factor that converts lb/ft^3 to kg/m^3 (Weast 1977)

The mass fraction of water vapor is (Çengel and Boles 1994,

$$f_{w.v.} = y_{w.v.}M_{w.v.} / M_{mix}$$

M_{mix} is the average molar mass of the mixture (kg/kmol), $y_{w.v.}$ is the mole fraction of water vapor, $M_{w.v.}$ is the molar mass of water vapor, 18.0153 g/mol (Weast 1977), and the following equations hold at station A:

$$P = 29.5300(16.018463\rho)R(273.15 + T_A)$$

$$M_{mix} = [(y_{air})(M_{air}) + (y_{w.v.})(M_{w.v.})]$$

$$y_{w.v.} = \frac{P_{w.v.}}{P}$$

$$y_{air} + y_{w.v.} = 1$$

$$RH = \frac{P_{w.v.}}{2.953\text{x}10^{-4}(1\text{x}10^3)P_{sat}(T_A)}$$

where R_o is the universal gas constant, 0.08314 bar·m^3/(kmol K) (Çengel and Boles 1994) and M_{air} is the average molar mass of air, 28.97 g/mol (Çengel and Boles).

Combining these equations yields

$$\dot{Q} = \frac{11.86P + 0.442P_{sat}(T_A)RH}{273.15 + T_A}\dot{V}\Delta T_{BC}$$

where $\Delta T_{BC} = T_C - T_B$

If there is no loss of mass down the test train (no leaks), the flowrate will be constant along the test train. In the development of the previous equation, measurements at Station A were used to determine the flow rates of dry air and water vapor as there were redundant sensors.

A comprehensive uncertainty analysis of the heat removal rates was performed in *Testing to Provide Data for Ventilation System Design: Phase I* (CRWMS M&O 2002a). As a brief summary, the uncertainties in the measured quantities used as inputs were considered as sources of uncertainty in the calculated heat removal rates. The effects of uncertainties in the temperatures at stations B and C, T_B and T_C, were not treated separately; instead, the temperature difference ΔT_{BC} was considered an input to the calculation. The approach permitted consideration of the effect of the subtraction on the systematic components of the measurement uncertainties. Once the heat removal rate and it's associated uncertainty has been determined, the ventilation efficiency can be calculated. The ventilation efficiency, η, is $\eta = \overline{\dot{Q}} / \overline{\dot{Q}_{in}}$, where $\overline{\dot{Q}}$ is the 24-hour average heat removal rate and $\overline{\dot{Q}_{in}}$ is the 24-hr average power generated in the waste packages.

The uncertainty of the calculated ventilation efficiency was determined using the law of propagation of uncertainties. It

was found that the uncertainty in the 24-hour average heat removal rate was dominated by the uncertainty in the volumetric flow rate (CRWMS M&O 2002a).

Tables 3 and 4 provides the calculated efficiencies and uncertainties for all of the Phase I and Phase II tests, respectively. The tables include the nominal power input and ventilating airflow rate. For the Phase II tests, the inlet temperature and inlet air relative humidity are also shown. It is important to note that the uncertainties shown in the tables reflect only the effects of the sensors and the calculation, not the test conditions, thus making direct comparisons difficult in some cases. During the Phase I tests the ventilating air (and hence all of the temperature measurements) showed a diurnal fluctuation based on the heating and cooling cycles of the experimental area. This fluctuation affected all heat transfer mechanisms within the test train. For the tests the daily ventilating air temperature typically oscillated 2-4C. However, the diurnal oscillation for test 4 was significantly higher (7C). In comparing the calculated efficiencies this test showed one of the lowest efficiencies. This is contradictory to what is expected (for a given power input the ventilation efficiency should increase with the ventilation flow rate). Because the inlet air conditions for the Phase II tests were controlled, calculated efficiencies can be directly compared. The observations from the efficiency calculations discussed below are based on results from the Phase II tests. In general, only changes in efficiency of 2-3% can be correlated to a given parameter. Changes smaller than this can be attributed to either slight variations in the other inputs that are assumed to be constant, or the uncertainty associated with each of the calculated efficiencies.

Table 3. Calculated efficiencies for the Phase I tests.

Test No.	Case No.	Target Flow Rate (m^3/s)	Target Power Input (W/m)	Ventilation Efficiency (Mixture) (%)	Uncertainty (%)
1	4	1.0	180	83.8	0.6
2	5	0.5	180	79	2
3	1	1.0	360	86.4	0.6
4	2	2.0	360	79.7	0.2
5	3	0.5	360	81	2
6	6	3.0	360	86.4	0.7

Effect of inlet air relative humidity on ventilation efficiency: Changes in relative humidity were found to have a negligible impact on ventilation efficiency. Subtle changes in comparable tests (tests 3 and 4, 7 and 8, 15 and 16) did not follow RH trends, i.e., an increase in RH does not result in an increase in efficiency. Slight changes in the calculated efficiencies can be attributed to differences in other conditions (i.e., inlet air temperature or airflow rate), and are within the error of the measurements. The tests that most clearly demonstrate the lack of effect on the ventilation efficiency by the relative humidity are 15 and 16. These tests had the largest change in RH (from ~32% to ~50%)

Table 4. Calculated efficiencies for the Phase II tests.

Test #	Target Power Level	Target Flow Rate	Inlet Air Temperature (Sta B)	Inlet air R.H. (Sta A)	Ventilation Efficiency (Mixture)	Uncertainty
	(kW/m)	(m3/s)	(°C)	(%)	(%)	(%)
1	0.22	1	24.5	29.6	93.9	0.7
2			34.2	18.8	79.9	0.6
3			44.4	10.2	75.9	0.5
4			44.1	14.5	74.9	0.5
5	0.36	1	25.1	29.0	92.7	0.6
6			34.8	17.1	89.4	0.6
7			44.4	9.8	81.0	0.6
8			44.3	14.5	81.4	0.6
9	0.22	0.5	25.3	30.1	92	3
10			34.9	16.6	82	2
11			44.5	16.3	72	2
12	0.36	0.5	26.3	29.7	91	3
13			34.9	16.5	81	2
14			44.6	9.7	73	2
15	0.36	1	29.6	32.3	90.3	0.6
16			29.2	49.5	90.9	0.6

while all other test conditions remained nearly constant. The calculated efficiency for test 15 (~32% RH) is 90.3% and for test 16 is 90.9%. Given the uncertainty in the efficiency calculation, these values are identical. Any actual difference in the efficiency could also stem from slight variations in the inlet temperature (test 16 has a measured inlet temperature 0.4 degrees cooler than test 15) or the power level. When evaluating the effects of other parameters on the ventilation efficiency, changes in the inlet air moisture content were neglected.

Effect of inlet temperature on ventilation efficiency: The inlet air temperature was found to be the largest contributing factor to the ventilation efficiency. As the inlet air temperature increased, the ventilation efficiency decreased. Neglecting changes in relative humidity, the effect of the inlet temperature on the ventilation efficiency can be seen in tests 1 through 4, 5 through 8, 9 through 11, and 12 through 14. At the lower flow rates (tests 9-11 and 12-14), the efficiency typically drops around 10%, for each 10 degree rise in the inlet air temperature. A similar trend can be seen in the high flow-rate tests (1-4, and 5-8). This effect is a function of the change in the ventilating air density as a function of temperature.

Effect of flow rate on ventilation efficiency: Higher flow rates generally result in higher efficiencies. The difference between the efficiencies is greater for tests with a higher heat input. Tests with lower heat input (and varying flow rates) had efficiencies varying less than 5%. Tests with higher heat input (and varying flow rates) had efficiencies varying between 8-9%.

Effect of power input on ventilation efficiency: At higher flow rates, the tests with higher heat input generally have higher efficiencies. One exception to the higher efficiencies at higher flow rates can be seen between tests 1 and 5. However, test 1 has a measured inlet temperature 0.6°C cooler than test 5, which may overshadow the effects of the power input. The effect of the power input on the ventilation efficiency at the lower flow rate is not conclusive. Efficiencies at the lower flow rate are within the uncertainty of the calculation, and do not appear to follow any dominant trend.

In the range of temperatures, flow rates, and power inputs represented in these tests, ventilation efficiency was most influenced by the inlet temperature, followed by the flow rate.

Conclusions and Discussion

A series of twenty-two ventilation tests were performed at the DOE Atlas testing facility. Data from the Phase I and Phase II Ventilation Test series were used to evaluate the ability of the ventilating air to remove energy under varying flow and input power conditions, as well as ventilating air temperature and relative humidity conditions. Results from this test series are applicable to the specific test configuration and conditions tested, for the purpose of validating codes and models.

The ventilation test series provided a range of flow and thermal conditions suitable for validation of heat and mass transport codes currently used by the YMP. Both steady-state and transient data was produced for comparison with ANSYS and FLUENT simulations, where temperature distributions and ventilation efficiencies will be compared with test results. Because of the heat transfer regime anticipated in both these tests and the full scale emplacement configuration (a combination of both forced and natural convection), the test results are also being used to validate mixed-convection analytic models.

Acknowledgements

The U.S. Department of Energy (DOE) Office of Civilian Radioactive Waste Management supported this work through its Office of Repository Development (ORD), formerly the Yucca Mountain Site Characterization Office (YMSCO).

References

Howard, C. 2001a. Preclosure Ventilation Test – 1/4-Scale. Scientific Notebook SN-SNL-SCI-020-V1. ACC: MOL.20010529.0267.

CRWMS M&O 2002a. *Testing to Provide Data for Ventilation System Design: Phase I.* TDR-EBS-MD-000024 REV 00. Las Vegas, Nevada: CRWMS M&O.

CRWMS M&O 2002b. *Testing to Provide Data for Ventilation System Design: Phase II.* TDR-EBS-MD-000024 REV 00. Las Vegas, Nevada: CRWMS M&O.

Cengel, Y. A. and Boles, M. A 1994. *Thermodynamics: An Engineering Approach.* 2nd Edition. San Francisco, CA: McGraw-Hill, Inc. TIC: 251427.

Weast, R.C., ed. 1977. *CRC Handbook of Chemistry and Physics.* 58th Edition. Cleveland, Ohio: CRC Press. TIC: 242376.